PIBB 生物化学与生物物理进展
Progress in Biochemistry and Biophysics
2021,48(12):1501~1507
www.pibb.ac.cn

Angiogram Deblurring in Absorption Intensity Fluctuation Modulation Imaging Using a Normalized Cross-correlation Algorithm*

WANG Xue-Hua[1,2)**], WENG Jia-Shun[1,2)**], WANG Ming-Yi[1,2)***], HUANG Li-Yuan[1,2)], XU Xiang-Cong[1,2)], HAN Ding-An[1,2)], ZENG Ya-Guang[1,2)***]

([1)]*School of Physics and Optoelectronic Engineering, Foshan University, Foshan* 528225, China;
[2)]*Guangdong-Hong Kong-Macao Joint Laboratory for Intelligent Micro-Nano Optoelectronic Technology, Foshan University, Foshan* 528225, China)

Abstract Full-field label-free optical angiography is a powerful imaging technique that aids study of cardiovascular diseases in live animal models. Here, we presented a novel method that combined absorption intensity fluctuation modulation imaging with sub-pixel matching based on a normalized cross-correlation algorithm to eliminate blurring of angiograms caused by system drift or biological jitter. Raw images showing absorption difference between red blood cells and background tissue under illumination with low-coherence light were captured and divided into several short image sequences. These sequences were then used for image reconstruction using absorption intensity fluctuation modulation imaging to achieve full-field angiography by isolating dynamic red blood cell signals from the background signal in the frequency domain. All the reconstructed images were then matched with the first reconstructed image using the normalized cross-correlation algorithm and subsequently fused. *In vivo* angiography near chicken embryo heart was performed to demonstrate the efficacy of our method, and it produced clear, blur-free angiograms with high spatial resolution and signal-to-noise ratio.

Key words absorption imaging, normalized cross-correlation, image matching, image analysis
DOI: 10.16476/j.pibb.2021.0012

Label-free optical angiography of live biological specimens[1-3] enables detection of the physiological mechanisms of various diseases linked to blood circulation systems[4-6]. Various optical imaging methodologies have recently been developed, such as optical coherence tomography angiography (OCTA) [7-9], full-field laser Doppler imaging[10-11], laser speckle contrast imaging[12-13], laser speckle imaging with intensity fluctuation modulation[14-15], and full-field functional optical angiography[16]. OCTA is widely used for vascular imaging in the eye[17], but the spot-scanning mode is time consuming and cannot simultaneously monitor the entire area in a frame. In comparison, the full-field methods have higher temporal resolution and ensure simultaneous acquisition of signal in each pixel, which is important for studying the blood microcirculation systems globally. Absorption intensity fluctuation modulation (AIFM) was proposed by Wang *et al*. previously[16]. It

* This work was supported by grants from The National Natural Science Foundation of China (61805038, 62075042, 61705036, 61771139) and Research Fund of Guangdong-Hong Kong-Macao Joint Laboratory for Intelligent Micro-Nano Optoelectronic Technology (2020B1212030010).

** These authors contributed equally to this work.
*** Corresponding author.
Tel: 86-757-82716895
WANG Ming-Yi. E-mail: wangmingyi@mail.bnu.edu.cn
ZENG Ya-Guang. E-mail: zeng.yg @163.com

Received: January 15, 2021 Accepted: April 9, 2021

achieved full-field blood flow measurement of near-transparent live animal models using modulation depth (MD) imaging and isolation of dynamic red blood cell (RBC) signal from the background signal, using an appropriate filter. However, as this method reconstructed blood flow images from sequences of raw images collected over a long period, the drift of biological samples caused by systemic factors or biological jitter during raw image acquisition can disrupt the quality of images of specific tissues, such as those of vessels near the heart, eyes, and brain. To resolve this issue, we aimed to develop a new method for AIFM imaging using a short-time normalized cross-correlation algorithm[18]. *In vivo* AIFM angiography of vessels near chicken embryo heart was performed to demonstrate that our method revealed the clear structure of blood vessels with higher spatial resolution and signal-to-noise ratio (*SNR*). Our method can thus potentially be used for *in vivo* dynamic angiography. Notably, the imaging modifications presented in our method are software-based and thus, economical.

1 Materials and methods

A schematic diagram of the experimental setup was shown in Figure 1a[16]. Low-coherence light from a light source (central wavelength λ_0=540 nm, a bandwidth of 10 nm, 100 mW) was used to illuminate the sample homogeneously in the form of an area source (LED). A chicken embryo placed in a custom container was used as the biological sample. It was developed for three days in an incubator at constant temperature (38℃) and humidity (60%). Before imaging, the following sample processing steps were performed: a part of the eggshell, shell membrane, and extraembryonic membrane above the yolk blood vessels and chicken embryo were successively and carefully removed. The main blood vessels near the chicken embryo heart (hereinafter called root blood vessels) were imaged, as they are significantly affected by the heartbeat. The diffuse reflected light was collected using a zoom bitelecentric lens and relayed onto a high-speed complementary metal-oxide semiconductor camera (CMOS) (Aca2000-340km, Basler, Germany). Using a pixel size of 5.5 μm × 5.5 μm, a sampling rate of 42 frames per second (fps), and an exposure time of 20 ms, 2 000 successive images were captured by the camera for blood flow visualization. The acquired image sequences were then transmitted to the host computer through a Camera Link high-speed frame grabber (PCIe-1433, National Instrument, USA). The system was fixed on a vibration-isolator optical platform in a darkroom. The embryo was carefully handled in accordance with the laboratory animal protocol approved by the Institutional Animal Care and Use Committee of Foshan University.

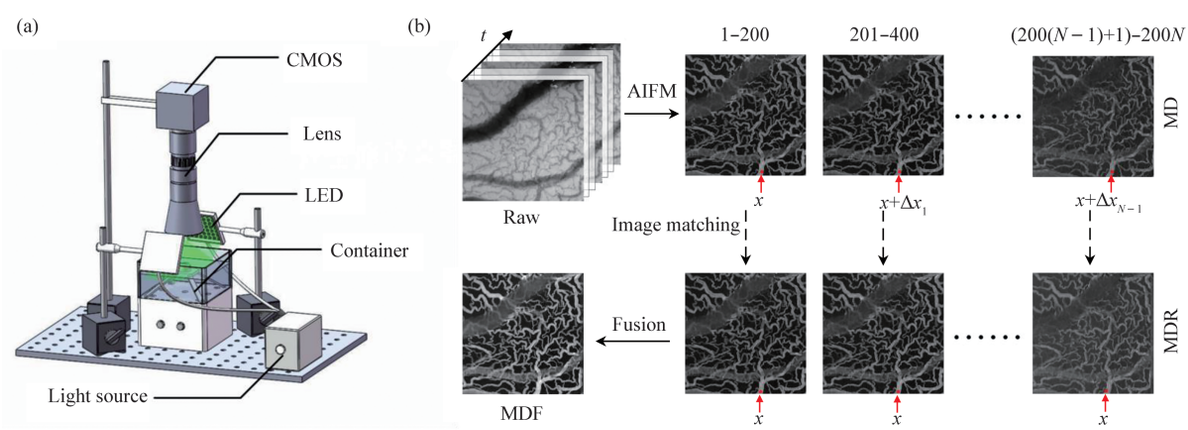

Fig. 1 Schematic diagram of the short−time normalized cross−correlation AIFM imaging setup

(a) Experimental device. (b) Data-processing method, in which the red arrows indicate the locations of the marked blood vessel. MDR and MDF represent modulation depth imaging after registration and fusion, respectively.

According to the AIFM imaging method[16], the raw temporal absorption signal recorded at each pixel was first transferred from the time domain to the frequency domain using a fast Fourier transform (FFT), in which the RBC and background signals were modulated to the high- (1.9 to 190 Hz) and low- (0 to 1.9 Hz) frequency ranges, respectively. Then, one of the two was obtained by filtering out the frequency signal corresponding to another pattern. Finally, by applying inverse FFT to both RBC and background signals, their mean intensities [$\bar{I}_{ac}(x,y)$, $\bar{I}_{dc}(x,y)$] in the time domain were obtained. The *MD*, defined as

$$MD(x,y)=\frac{\bar{I}_{ac}(x,y)}{\bar{I}_{dc}(x,y)}, \tag{1}$$

is used to reconstruct an image of blood flow.

The AIFM method reconstructed blood flow images from a sequence of raw images obtained over a long period. To alleviate the blurring of angiograms caused by system drift or biological jitter during raw image acquisition, we proposed a novel method for short-time normalized cross-correlation AIFM imaging. As shown in Figure 1b, raw images were divided into several smaller sets and reconstructed separately using the AIFM algorithm. All the reconstructed images were then matched with the first reconstructed image and subsequently fused (final image).

We implemented the sub-pixel precision image registration algorithm using normalized cross-correlation[18-19]. According to theory, an image $g(x,y)$ of an object $f(x,y)$ can be reconstructed numerically from measurements of the magnitude of the Fourier transform of $f(x,y)$. The quality of the reconstruction can be assessed through an error metric that is invariant to these operations. One such metric is the normalized root-mean-square error (NRMSE) E between $f(x,y)$ and $g(x,y)$, defined by

$$\begin{aligned}E^2&=\min_{\alpha,x_0,y_0}\frac{\sum_{x,y}\left|\alpha g(x-x_0,y-y_0)-f(x,y)\right|^2}{\sum_{x,y}\left|f(x,y)\right|^2}\\&=1-\frac{\max\left|r_{fg}(x_0,y_0)\right|^2}{\sum_{x,y}\left|f(x,y)\right|^2\cdot\sum_{x,y}\left|g(x,y)\right|^2},\end{aligned} \tag{2}$$

where summations are taken over all image points (x,y), and

$$\begin{aligned}r_{fg}(x_0,y_0)&=\sum_{x,y}f(x,y)\,g^*(x-x_0,y-y_0)\\&=\sum_{u,v}F(u,v)\,G^*(u,v)\exp\left[i2\pi\left(\frac{ux_0}{M}+\frac{vy_0}{N}\right)\right],\end{aligned} \tag{3}$$

is the cross-correlation of $f(x,y)$ and $g(x,y)$, N and M are the image dimensions, $*$ denotes complex conjugation, and uppercase letters represent the discrete Fourier transform of their lowercase counterparts, as given by the relation

$$F(u,v)=\sum_{x,y}\frac{f(x,y)}{\sqrt{MN}}\exp\left[i2\pi\left(\frac{ux}{M}+\frac{vy}{N}\right)\right]. \tag{4}$$

Thus, evaluation of the NRMSE using Equation (2) requires solving the more general problem of sub-pixel image registration by locating the peak of the cross-correlation$r_{fg}(x,y)$.

Notably, the influence of sample drift on each MD image was relatively small, and even neglected, over a short period. However, the position offset between every MD image was corrected using the normalized cross-correlation algorithm. As shown in Figure 1b, the blood vessel position offsets marked by red arrows in the MD images were effectively corrected in the MD registration (MDR) images, proving that our method can be used to improve angiogram quality.

To quantitatively assess the calibration capability of the proposed method, sample drift traces and drift-corrected traces of the x and y directions[20] were determined, as shown in Figure 2a. Both traces were precisely calibrated, and the means of corrected drift errors were 0 μm and 0.55 μm for the x and y directions, respectively. This verified the sub-pixel precision (pixel size of 5.5 μm) of the image registration algorithm using normalized cross-correlation. Additionally, to find the optimal step length for AIFM angiogram reconstruction, the means of corrected drift errors with different step lengths were calculated, as shown in Figure 2b, which yielded a minimum of approximately 200 frames. Therefore, we divided the 2 000 raw images into 10 smaller blocks of 200 frames each for image reconstruction in this study.

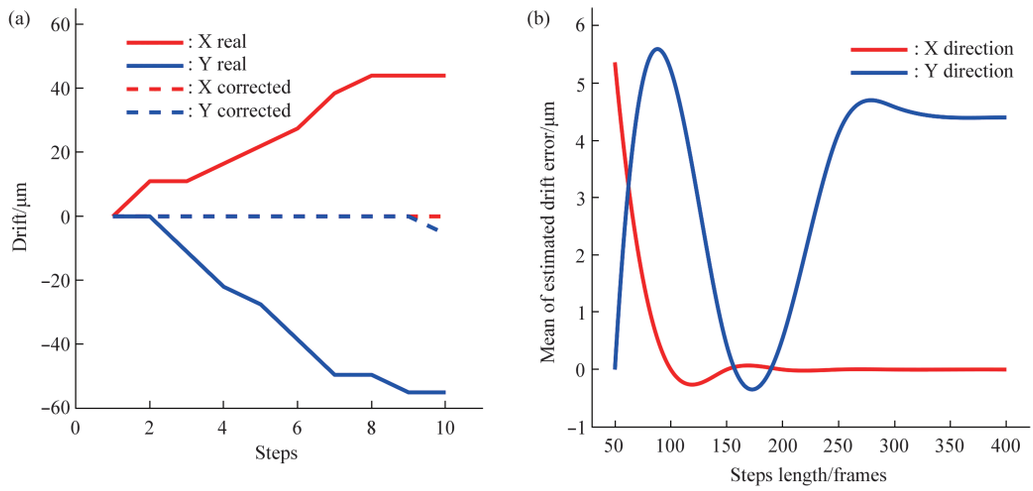

Fig. 2　Drift correction precision achieved using the proposed method

(a) Sample drift traces and drift-corrected traces in the *x* and *y* directions. (b) Means of drift correction errors for 2 000 raw images with different step lengths. The values reached a minimum of around 200 frames for both *x* and *y* directions.

2　Results and discussion

The feasibility of our method is shown in Figure 3. Figure 3a presented the raw MD images reconstructed from 2 000 images. Owing to significant jitter caused by the heartbeat of the chicken embryo, the raw MD image clarity was poor,

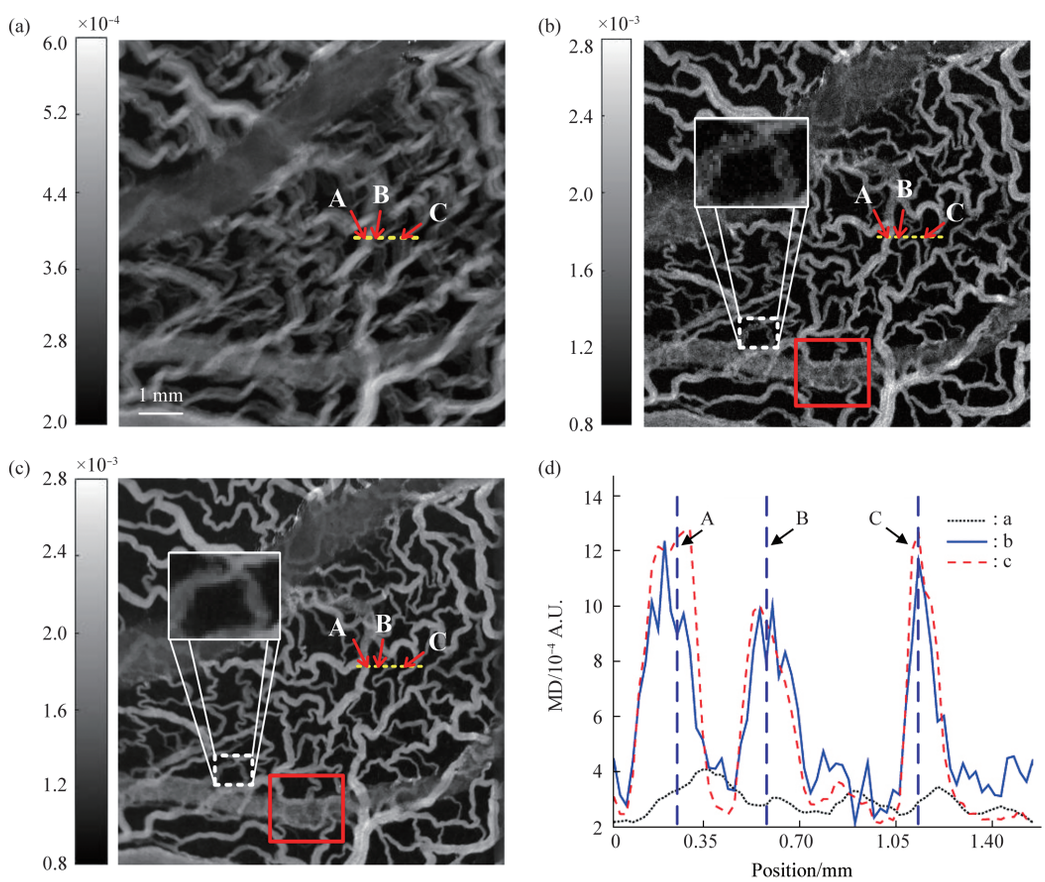

Fig. 3　Comparison of angiogram images reconstructed by different algorithms

(a) Raw MD, (b) the first short-time MD, and (c) MDF images. (d) MD signals of blood vessels marked by yellow dotted lines in images (a−c). A, B, and C represent the three signal peaks of blood vessels, respectively. The imaged area is 9.2 mm × 9.2 mm, and the magnification is 2-fold.

and the borders of the root blood vessels and capillaries were unclear. As the influence of sample drift over a short period can be neglected, the first short-time MD image reconstructed from 1−200 images was shown in Figure 3b, which presented a clearer vascular structure than the raw MD image. However, owing to the use of too few raw images for reconstruction, the borders of the root blood vessels and capillaries were not smooth. The MD images reconstructed from data sequences collected over a short period did not provide satisfactory angiograms. However, they could be used to calibrate the locations of blood vessels. Therefore, the MDR image was obtained by matching every MD image with the first image using the normalized cross-correlation algorithm. Ten MDR images were fused to obtain the final angiogram (MD fusion, MDF) shown in Figure 3c. The results demonstrated better clarity and blood vessel integrity than those for the other two.

Reflecting the advantages of our method, Figure 3d showed the signals of the vessels marked A, B, and C obtained from the images presented in Figure 3a−c. The peaks of the three lines in Figure 3d represented the vessels marked A, B, and C, respectively. The borders of the vessels shown in Figure 3c were clearer and smoother than those of the vessels shown in Figure 3a and 3b. Additionally, as shown in the enlarged view of the area marked by the white box in Figure 3b and 3c, the vessels border shown in Figure 3c was more continuous, with richer vessel information than that seen in Figure 3b. In the area marked by the red box in Figure 3c, the capillaries covered by the main blood vessels were clearer and more complete than that in Figure 3b.

Next, the feasibility of our method was assessed quantitatively (Figure 4). The raw MD and MDF images were shown in Figure 4a and 4b, respectively. Two differently colored dotted lines were used to mark the same area in the two images. The parameters of location spatial resolution and *SNR*[21] calculated from the seven yellow and red dotted lines in the marked area were used to evaluate image quality. The

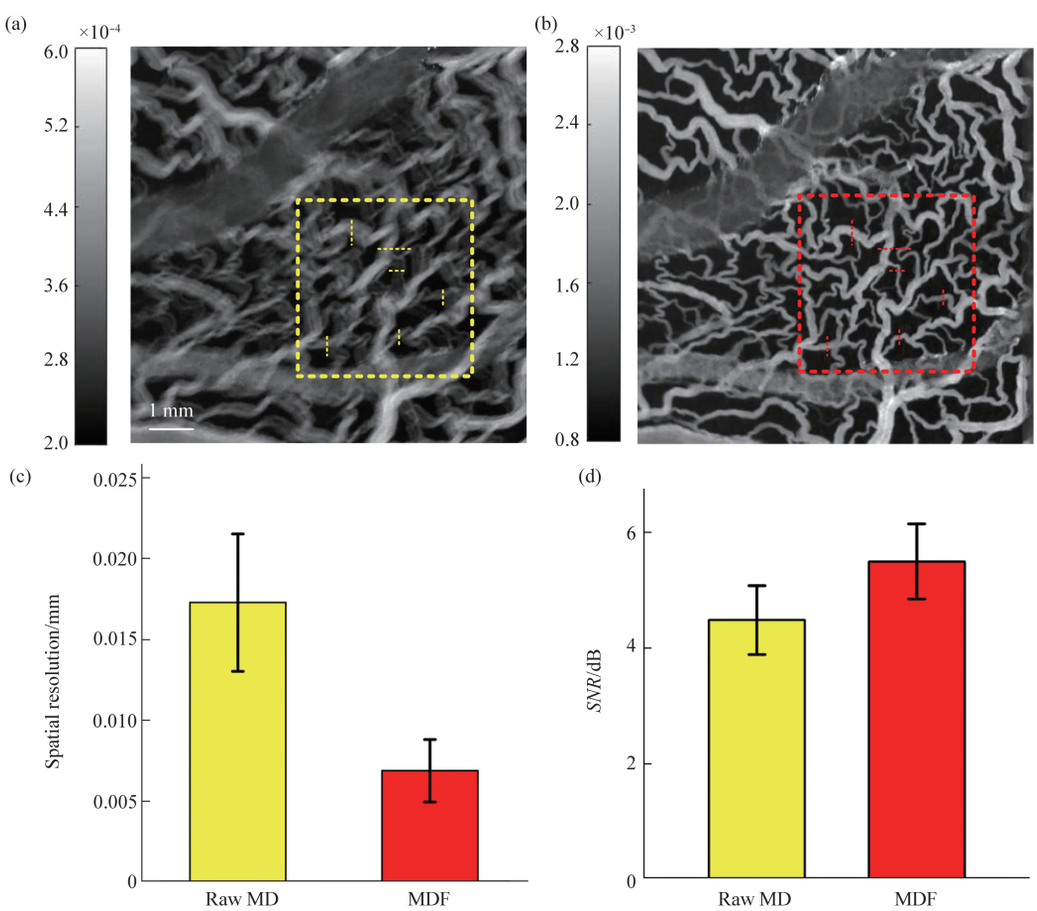

Fig. 4　Quantitative comparison of spatial resolution and *SNR* in different angiogram images

(a) Raw MD and (b) MDF images. (c) Comparison of spatial resolutions. (d) Comparison of *SNR*.

former was defined as the difference between the full widths at one-fourth maximum and full widths at half maximum of the blood flow peak intensity, and the latter was defined as

$$SNR = 20\ln(I/S) \quad (5)$$

where I and S are the blood flow peak intensity and background intensity, respectively. Compared with the results presented in Figure 4c and 4d, those in Figure 4b showed a higher spatial resolution and *SNR* than those shown in Figure 4a, indicating that the proposed method offered higher angiogram image quality.

3 Conclusion

We proposed here a modified short-time normalized cross-correlation AIFM imaging method to improve image acquisition for angiography. We verified our method by performing *in vivo* angiography of vessels near a chicken embryo heart. The resulting images had high spatial resolution and *SNR*. Our method can be used to correct the angiogram blur caused by heartbeat, respiration, subtle eye motions, and nervous tremor of near-transparent live animal models, such as younger embryos, macula lutea, and zebra fish. It can also potentially be applied in the study of the physiological mechanisms underlying several diseases related to the cardiovascular system.

References

[1] Doh I, Yoo H I, Cho Y H, *et al*. Viable capture and release of cancer cells in human whole blood. Appl Phys Lett, 2012, **101**(4):375-377

[2] Rodrigues S F, Vital S A, Granger D N. Mild hypercholesterolemia blunts the proinflammatory and prothrombotic effects of hypertension on the cerebral microcirculation. J Cereb Blood Flow Metab, 2013, **33**(4):483-489

[3] Koller A, Balasko M, Bagi Z. Endothelial regulation of coronary microcirculation in health and cardiometabolic diseases. Intern Emerg Med, 2013, **8**(Suppl 1):S51-S54

[4] Burgansky-Eliash Z, Barak A, Barash H, *et al*. Increased retinal blood flow velocity in patients with early diabetes mellitus. Retina, 2012, **32**(1):112-119

[5] Burgansky-Eliash Z, Nelson D A, Bar-Tal O P, *et al*. Reduced retinal blood flow velocity in diabetic retinopathy. Retina, 2010, **30**(5):765-773

[6] Coverdale N S, Gati J S, Opalevych O, *et al*. Cerebral blood flow velocity underestimates cerebral blood flow during modest hypercapnia and hypocapnia. J Appl Physiol, 2014, **117**(10):1090-1096

[7] Mariampillai A, Standish B A, Moriyama E H, *et al*. Speckle variance detection of microvasculature using swept-source optical coherence tomography. Opt Lett, 2008, **33**(13):1530-1532

[8] June C W, Li Y, Wan Q, *et al*. Cerebral capillary velocimetry based on temporal OCT speckle contrast. Biomed Opt Express, 2016, **7**(12):4859-4873

[9] Chu Z, Lin J, Chen G, *et al*. Quantitative assessment of the retinal microvasculature using optical coherence tomography angiography. J Biomed Opt, 2016, **21**(6):66008

[10] Serov A, Steinacher B, Lasser T. Full-field laser Doppler perfusion imaging and monitoring with an intelligent CMOS camera. Opt Express, 2005, **13**(10):3681-3689

[11] Serov A, Lasser T. High-speed laser Doppler perfusion imaging using an integrating CMOS image sensor. Opt Express, 2005, **13**(17):6416-6428

[12] Freund I. Joseph W. Goodman: speckle phenomena in optics: theory and applications. J Stat Phys, 2008, **130**(2):413-414

[13] Murari K, Li N, Jia A R X, *et al*. Contrast-enhanced imaging of cerebral vasculature with laser speckle. Appl Opt, 2007, **46**(22): 5340-5346

[14] Zeng Y, Wang M, Feng G, *et al*. Laser speckle imaging based on intensity fluctuation modulation. Opt Lett, 2013, **38**(8):1313-1315

[15] Wang M, Zeng Y, Liang X, *et al*. Full-field optical micro-angiography. Appl Phys Lett, 2014, **104**(5): 053704

[16] Wang M, Mao W, Guan C, *et al*. Full-field functional optical angiography. Opt Lett, 2017, **42**(3):635-638

[17] Guizar-Sicairos M, Thurman S T, Fienup J R. Efficient subpixel image registration algorithms. Opt Lett, 2008, **33**(2):156-158

[18] Matthias B, Vito R, Bernhard S, *et al*. Imaging of corneal neovascularization: optical coherence tomography angiography and fluorescence angiography. Invest Ophthalmol Vis, 2018, **59**(3):1263-1269

[19] Debella-Gilo M, Kääb A. Sub-pixel precision image matching for measuring surface displacements on mass movements using normalized cross-correlation. Remote Sens Environ, 2011, **115**(1): 130-142

[20] Tang Y, Wang X, Zhang X. Sub-nanometer drift correction for super-resolution imaging. Opt Lett, 2014, **39**(19):5685-5688

[21] Wang Y, Li C, Wang R K. Noncontact photo acoustic imaging achieved by using a low-coherence interferometer as the acoustic detector. Opt Lett, 2011, **36**(20):3975-3977

利用归一化互相关算法去除吸收强度涨落调制血管造影图像模糊*

王雪花[1,2)**]　翁嘉瞬[1,2)**]　王茗祎[1,2)***]　黄丽媛[1,2)]　许祥丛[1,2)]　韩定安[1,2)]　曾亚光[1,2)***]

（[1)] 佛山科学技术学院物理与光电工程学院，佛山 528225；

[2)] 佛山科学技术学院粤港澳智能微纳光电技术联合实验室，佛山 528225）

摘要　吸收强度涨落调制成像（AIFM）方法是基于血红细胞和背景组织对低相干光照明的吸收差异，通过在频域分离动态的血红细胞信号和静态的背景信号，实现对近透明活体生物样本全场无标记的光学血管造影成像. 但此成像方法需采集较长的原始图像序列，系统漂移或生物抖动会造成图像模糊，难以实现对某些特定区域的血管造影成像. 本文提出一种结合AIFM成像和归一化互相关算法的新方法来提升血管造影图像的质量：原始的图像序列被分成若干短时序列，每个短时序列先利用AIFM成像算法重构得到全场的血管造影图像；再利用归一化的互相关算法将所有的短时重构图像与第一帧重构图像相匹配，并融合得到最终的血管造影片. 我们以活体鸡蛋胚胎为样品，通过实验验证了利用短时归一化互相关AIFM成像方法，能够消除鸡胚胎心跳引起的图像模糊，从而获得高分辨率和信噪比的心血管造影片，对研究活体动物心脑血管疾病具有重要应用价值.

关键词　吸收成像，归一化互相关，图像匹配，图像分析

中图分类号　Q445　　**DOI**：10.16476/j.pibb.2021.0012

* 国家自然科学基金（61805038，62075042，61705036，61771139），粤港澳智能微纳光电技术联合实验室（2020B1212030010）资助项目.

** 并列第一作者.

*** 通讯联系人.

Tel：0757-82716895

王茗祎. E-mail：wangmingyi@mail.bnu.edu.cn

曾亚光. E-mail：zeng.yg@163.com

收稿日期：2021-01-15，接受日期：2021-04-09